A modeling study of the role that bottom topography plays in Gulf Stream dynamics and in influencing the tilt of mean sea level along the US East Coast

Tal Ezer[1]

Abstract Two aspects of the interactions between the Gulf Stream (GS) and the bottom topography are investigated: 1. the spatial variations associated with the north-south tilt of mean sea level along the US East Coast and 2. the high-frequency temporal variations of coastal sea level (CSL) that are related to Gulf Stream dynamics. A regional ocean circulation model is used to assess the role of topography; this is done by conducting numerical simulations of the GS with two different topographies–one case with a realistic topography and another case with an idealized smooth topography that neglects the details of the coastline and the very deep ocean. High-frequency oscillations (with a 5-day period) in the zonal wind and in the GS transport are imposed on the model; the source of the GS variability is either the Florida Current (FC) in the south or the Slope Current (SC) in the north. The results demonstrate that the abrupt change of topography at Cape Hatteras, near the point where the GS separates from the coast, amplifies the northward downward mean sea level tilt along the coast there. The results suggest that idealized or coarse resolution models that do not resolve the details of the coastline may underestimate the difference between the higher mean sea level in the South Atlantic Bight (SAB) and the lower mean sea level in the Mid-Atlantic Bight (MAB). Imposed variations in the model's GS transport can generate coherent sea level variability along the coast, similar to the observations. However, when the bottom topography in the model is modified (or not well resolved), the shape of the coastline and the continental shelf influence the propagation of coastal-trapped waves and impact the CSL variability. The results can explain the different characteristics of sea level variability in the SAB and in the MAB and help understand unexpected water level anomalies and flooding related to remote influence of the GS.

1 Introduction

The dynamics of the Gulf Stream (GS) is closely connected with the topography of the region. Flow-bathymetry interactions may involve both coastal dynamics associated with the shape of the coastline or the continental shelf and slope (e.g., Xue and Oey 2011), or deep ocean dynamics associated for example with the passage of the GS over the New England Seamounts (Ezer 1994). Past ocean modeling studies of the region often focus on ocean circulation aspects such as the influence of topography on the Gulf Stream separation from the coast (there are too many studies on the subject to list, but see summary in recent studies; Ezer 2016a, Schoonover et al. 2017). The GS-topography interaction may also affect two interesting aspects of coastal sea level with a long history of research (Montgomery 1938; Sturges 1974). The two issues addressed here are 1. the spatial variations of north-south tilt of mean sea level along the coast and 2. GS-related temporal variations in coastal sea level. The attention given now to climate change and sea level rise renews the interest in those old problems (e.g., see Higginson et al. 2015 and Ezer 2016b,

for review of problems 1 and 2, respectively). Both the spatial sea level tilt and the temporal variations show clear distinction between the coastal sea level dynamics in the South Atlantic Bight (SAB) and that in the Mid-Atlantic Bight (MAB). Moreover, long-term climatic changes and sea level rise also show large differences between the MAB and the SAB, with a distinct acceleration of sea level rise north of Cape Hatteras (Sallenger et al. 2012; Boon 2012; Ezer 2013; Yin and Goddard 2013). These changes in coastal sea level along the US East coast suggest that the GS dynamics and its interaction with the changing topography along its path may play an important role (though Woodworth et al. 2014 suggested a lesser role for the GS and a larger role for wind). From the Florida Current (FC) in the Florida Straits, the GS is transformed to a near-coast current flowing north in relatively shallow waters in the SAB, until it separates from the coast at Cape Hatteras and becomes a meandering current over deep waters in the MAB. In the MAB, the northern recirculation gyre separates between the GS and the coast with additional influence from the equatorward-flowing Slope Current (SC) and the Deep Western Boundary Current (DWBC) (Hogg 1992; Rossby et al. 2010). How do these differences in GS dynamics and topography between the SAB and MAB influence sea level along the coast is the main issue addressed here. It is worth noting, however, that in addition to GS-related dynamic influence on coastal sea level (CSL), variations in atmospheric pressure and wind can also have a significant influence, especially on interannual to decadal variability of sea level (Piecuch and Ponte 2015; Piecuch et al. 2016; Woodworth et al. 2014), as well as large-scale variations in the Sverdrup transport (Thompson and Mitchum 2014). The combination of variations in wind patterns and the North Atlantic Oscillations (NAO) may result in a different response between the coasts north of Cape Hatteras (MAB and GOM in Fig. 1) and the coasts south of Cape Hatteras (SAB) (Woodworth et al. 2016). The CSL in the SAB may be more closely related to variations in the NAO and the subtropical gyre circulation, and these variations can be monitored by the FC measurements (Baringer and Larsen 2001).

The hypothesis that some CSL variations along the US East Coast may relate to variations in the Atlantic Ocean circulation and the Gulf Stream (GS) has been suggested by early observations (Montgomery 1938; Blaha 1984) and some models (Ezer 2001; Ezer 2016b). Interestingly enough, GS-related CSL variability can be found on a wide range of time scales, from daily to weekly variations (Ezer and Atkinson 2014; Ezer 2016b) into decadal variations (Ezer et al. 2013; Ezer, 2013), and even long-term sea level rise may have contribution from potential slowdown of the GS (Sallenger et al. 2012; Ezer et al., 2013; Yin and Goddard 2013). In all those processes, a weakening in the GS flow and the sea level gradient across the GS is expected to cause anomalously higher sea level along the coast, as the onshore/offshore side of the

GS rise/fall. As a result, on one hand, observed sea level from tide gauges can be used to detect changes in the GS and the Atlantic Meridional Overturning Circulation (AMOC) (Ezer 2015), but on the other hand, observed variations in the GS transport from satellite altimeters or the cable data across the Florida Strait can be used to predict coastal sea level anomalies and tidal flooding (Ezer et al. 2013; Ezer and Atkinson 2014). The mechanism of remote forcing of the GS and CSL is complex (e.g., Domingues et al. 2016), not completely understood, and involves both large-scale dynamics and costal-trapped waves (Huthnance 2004; Ezer 2016b). However, this GS-related CSL variability process can be simulated, as demonstrated in the simplified and controlled model experiments of Ezer (2016b). However, the latter study used an idealized model with a smooth topography and a simplified coastline, so here this simplified model is compared with simulations using a more realistic topography to better understand the role that bottom topography plays in the GS dynamics and in CSL variations.
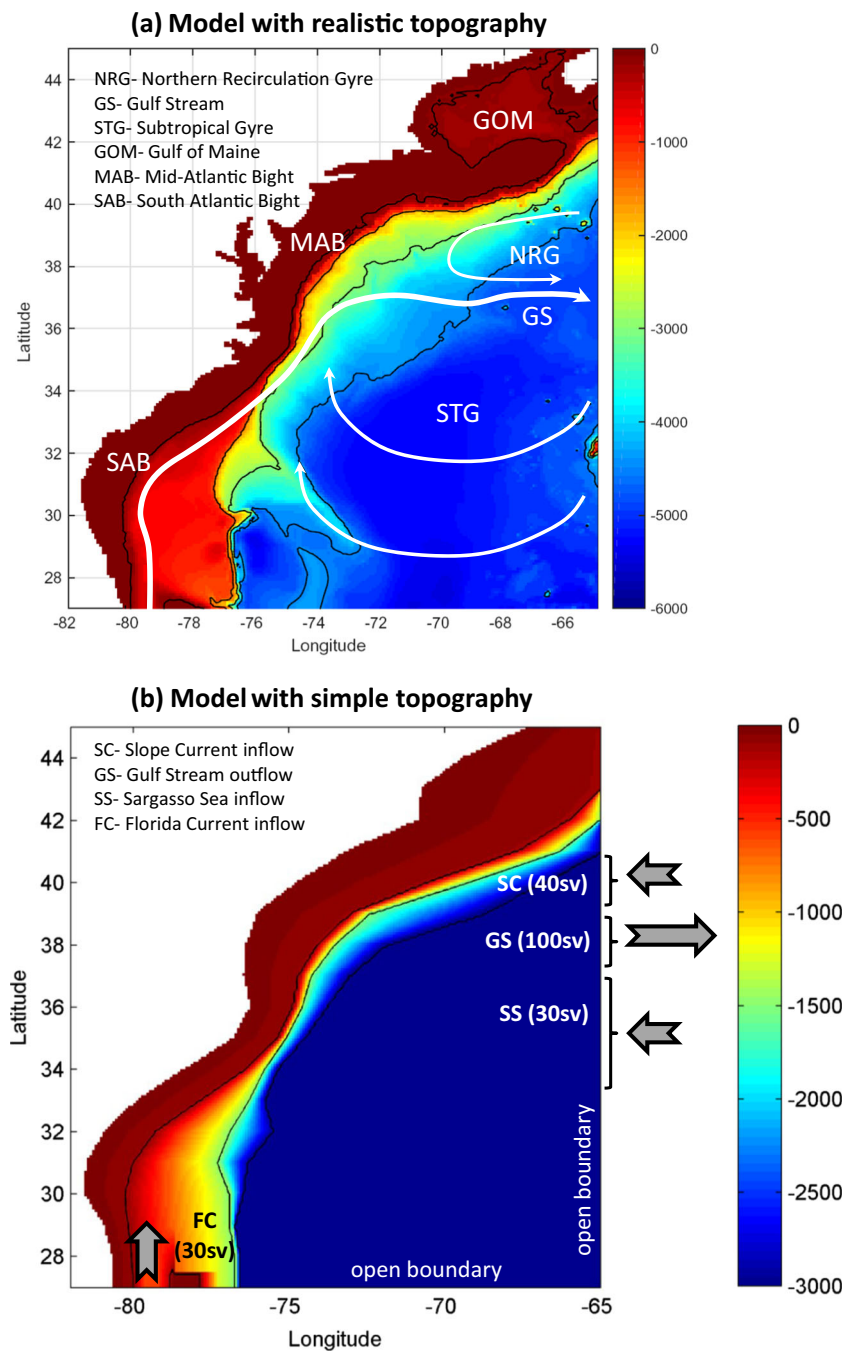
By comparing an idealized topography GS model with a more realistic model, it is also possible to address another issue–the role of topography in the downward tilt of mean sea level as one travels northward along the coast. This comparison has implications for coarse resolution models that do not resolve the details of the coastline near Cape Hatteras where the GS separates from the coast. Disagreements on the direction and size of this tilt between early geodetic leveling measurements and ocean dynamics (Sturges 1974) have been settled to some degree, though the issue is still of large interest. For example, recent comparisons between several modern geodetic models and several ocean circulation models show a considerable agreement; however, the same study casts some doubt on the role of this tilt in explaining the link between the GS and sea level rise in some climate models (Higginson et al. 2015). Here, the results of the models in Higginson et al. are compared with an idealized ocean circulation model running with different topographies to evaluate the role of the GS-topography interaction.

The paper is organized as follows. First, the model setup and the experiments are described in Section 2, then the results from different simulations are analyzed in Section 3, and finally discussions and conclusions are offered in Section 4.

2 Numerical model setup and experiments

The idealized regional numerical ocean model (Fig. 1b) and its setup are similar to the recent model of Ezer (2016a, b), but with additional experiments using a more realistic topography from the ETOPO5 dataset (Fig. 1a). The numerical code is based on the generalized coordinate ocean circulation model of Mellor et al. (2002), which includes a terrain-following vertical grid, a Mellor-Yamada turbulence scheme and

Fig. 1 **a** Bottom topography (color; depth in m) of the model ("realistic" model cases) obtained from ETOPO5; major currents and sub-regions are indicated. **b** The idealized topography ("simple" model cases) and the mean inflow/outflow boundary conditions (transport in Sv = 10^6 m^3 s^{-1}); inflows include the Florida Current (FC), the Slope Current (SC), and the Sargasso Sea (SS), and the outflow is the Gulf Stream (GS). The shown transport values are means, while the variations in the flow for different experiments are listed in Table 1. Bottom topography contours (*black lines*) are shown for depths of 100, 1500, 3000, and 4500 m; note the difference in maximum depth between **a** and **b**

(a) Model with realistic topography

NRG- Northern Recirculation Gyre
GS- Gulf Stream
STG- Subtropical Gyre
GOM- Gulf of Maine
MAB- Mid-Atlantic Bight
SAB- South Atlantic Bight

(b) Model with simple topography

SC- Slope Current inflow
GS- Gulf Stream outflow
SS- Sargasso Sea inflow
FC- Florida Current inflow

Smagorinsky-type horizontal diffusion. The main difference between the two configurations is that in the idealized case (Fig. 1b), detailed coastline features are eliminated, the bathymetry is smoothed, and the maximum depth is set to 3000 m (saving considerable computations). Therefore, the shape of the continental shelf and slope are different in the two cases. The minimum depth is set to 10 m in both cases. While the main focus of the study is on CSL in shallow waters, it will be interesting to see if the topography of the deep ocean has any indirect affect on the coastal dynamics. The model is driven at the surface by a constant monthly mean wind (May 2012, as in Figure 3 of Ezer 2016b), except experiments with oscillatory zonal wind as described below. Choosing a different month for the wind and the initial conditions (not shown) made insignificant impact on the results, since these are sensitivity experiments that do not attempt to exactly mimic the real ocean at a particular time. Surface heat and freshwater fluxes are set to zero. Inflow/outflow transports are imposed on the eastern and southern open boundaries as vertically averaged velocities at fixed locations (Fig. 1b), except cases with oscillatory transports, as described below. Note however that the fixed location of the GS outflow

(Fig. 1b) may reduce the model variability compared with the real ocean. Internal velocities at each level near the boundaries are free to adjust by the model's dynamics. The horizontal grid is a Cartesian grid with 1/12° resolution (~6–8 km grid size), and the vertical depth-scaled grid has 21 layers with higher resolution near the surface (e.g., the thickness of each layer varies from ~1/1000th to 1/15th of the water depth between the surface and bottom layers). Experiments in Ezer (2016a) with a much higher vertical resolution show a significant impact on the model results when a z-level grid is used, but very small impact when a terrain-following grid is used, as the case here. The three imposed inflow transports are the Florida Current (FC), the Slope Current (SC), and the Sargasso Sea (SS) and their total transport is equal to the outflow of the GS, as seen in Fig. 1b (see Ezer 2016a, b, for more details on the open boundary conditions). As in Ezer (2016b), the initial condition is the monthly mean temperature and salinity field for May 2012, derived from the ARMOR3D global reanalysis (Larnicol et al. 2006) and distributed by the EU-funded Copernicus Marine Environmental Monitoring Service (http://marine.copernicus.eu). For comparisons with the model results, sea surface height (SSH) from altimeter data is also used; the altimeter data were formerly distributed by AVISO (http://las.aviso.oceanobs.com; Ducet et al. 2000) but now are distributed by the Marine Copernicus site mentioned above. The main interest of the study is the short-term variability (hours to weeks), so the start of the simulations is not so important, as long as a quasi-realistic-looking GS is obtained after the initial adjustment, which achieved within days (see Fig. 2 in Ezer 2016a) when starting from a realistic density field and using imposed forcing for this small domain. The presented results are from the month after a 60-day spin up.

Eight different simulations are conducted and summarized in Table 1, four experiments with simple topography (marked "S"), and four experiments with real topography ("R"). The output fields are saved at 6-h intervals. The control experiments with constant forcing (wind and transport) have no imposed variability (NOVAR) except natural variations in the GS as it meanders or shed eddies, while in the other experiments, a 5-day-cycle sinusoidal forcing is imposed on zonal wind (WINDVAR), Florida Current inflow transport (FCVAR), and Slope Current inflow transport (SCVAR); the result of the variable inflow is a GS with outflow transport variations of 100 ± 10 Sv (1 Sv $= 10^6$ m^3 s^{-1}). Note that only the total barotropic inflow/outflow transports are varied. Based on the previous experiments of Ezer (2016b) that tested oscillations with periods between 2 and 10 days, the 5-day test case was selected here, as it closely resembles the observed variability.

3 Results

3.1 The impact of topography on the Gulf Stream dynamics

Despite the simplicity of the model and forcing, the simulated GS captures most of the characteristics of the GS as observed by many studies (Richardson and Knauss 1971; Hogg 1992; Johns et al. 1995; Rossby et al. 2010). Model velocity cross section across the GS has been compared with the observations of Richardson and Knauss (1971) and show reasonable agreement with the data despite the simplicity of the model (Fig. 3 in Ezer 2016b). Further comparisons of the model with SSH from altimeter data are shown in Fig. 2. Instantaneous sea surface height indicates a smoother and more zonal GS path in the case with a simple topography (Fig. 2a) and more GS meandering in the realistic case (Fig. 2c). This result is likely due to the lack of topographic variability in the deep ocean in NOVAR-S and is consistent with other modeling studies that show for example how the New England Seamount Chain increases the variability of the GS when it crosses over the seamounts (Ezer 1994). North-south cross sections across the GS in the MAB show quite realistic surface slope of 1–1.3 m over 100–200 km in both runs, but with somewhat larger changes in the slope amplitude in NOVAR-S (Fig. 2b) and more lateral shift in the GS position in NOVAR-R (Fig. 2d). The simulation with realistic topography

Table 1 Summary of model experiments. Inflow (+) and outflow (−) boundary conditions are specified for Florida Current (FC), Slope Current (SC), Sargasso Sea (SS), and Gulf Stream (GS); see Fig. 1b. The experiments with variable forcing use sinusoidal function with a 5-day period

Experiment	Transports (Sv)				Wind	Model topography
	FC	SC	SS	GS		
NOVAR-S	+30	+40	+30	−100	Monthly mean	Simple
NOVAR-R	+30	+40	+30	−100	Monthly mean	Real
WINDVAR-S	+30	+40	+30	−100	$U = \pm5$ m/s, $V = 0$	Simple
WINDVAR-R	+30	+40	+30	−100	$U = \pm5$ m/s, $V = 0$	Real
FCVAR-S	+30 ± 10	+40	+30	−100 ± 10	Monthly mean	Simple
FCVAR-R	+30 ± 10	+40	+30	−100 ± 10	Monthly mean	Real
SCVAR-S	+30	+40 ± 10	+30	−100 ± 10	Monthly mean	Simple
SCVAR-R	+30	+40 ± 10	+30	−100 ± 10	Monthly mean	Real

Fig. 2 Examples of instantaneous sea surface height (SSH) fields (*left panels*) and north-south cross sections of sea level across the Gulf Stream (*right panels*). The top two panels are the model simulations 30 days after the initial adjustment run for the simple topography (NOVAR-S case; *top panels*) and for the real topography (NOVAR-R case; *middle panels*). The *bottom panels* are examples of altimeter data for 25 May 2012. In the cross sections, *different color lines* represent different longitudes from 66°W to 74°W. The signature of features such as the Gulf Stream, cold-core eddy, northern recirculation, and southern recirculation gyres are indicated in **b**
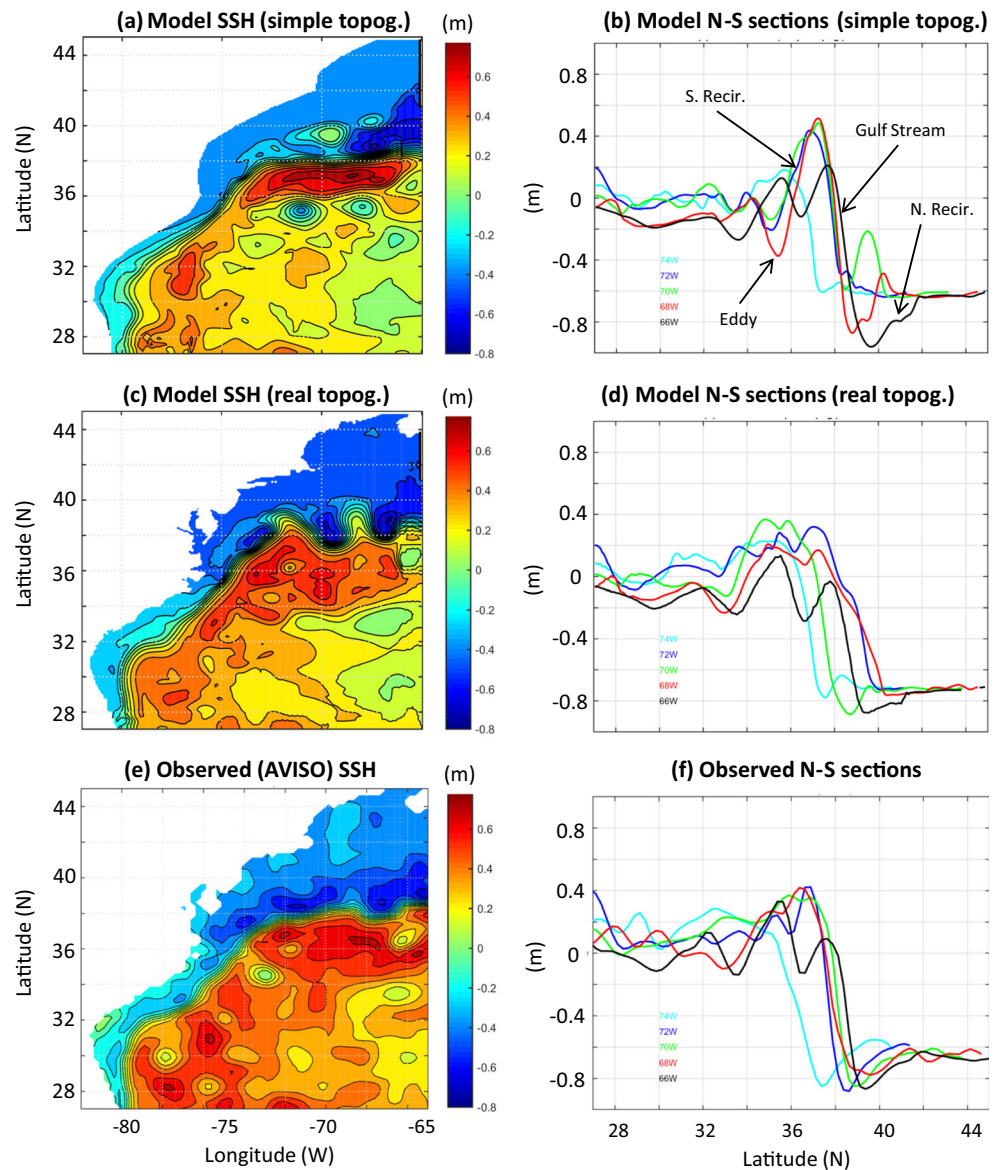

(Fig. 2d) more closely resembles the observed sea level section (Fig. 2f) than the idealized case do (Fig. 2b). Note that although the altimeter data obtained for 25 May 2012 represents similar time as that used for wind and initial condition in the model, one does not expect the mesoscale eddies and GS meandering to be similar to the model without data assimilation. In addition, the altimeter data is based on the one fourth degree gridded analysis, which has lower resolution than the model grid; this may explain the smooth nature of the altimeter SSH (Fig. 2e) compared with the model (Fig. 2c). Velocity cross sections in the MAB (Fig. 3a, b) show a quite realistic GS that captures the top 1000 m of the water column, and eastward flowing Slope Current along the continental slope (see Figure 3 in Ezer 2016b for further model-data comparisons). Neglecting the deep ocean (Fig. 3a) had little effect on the basic structure of the GS. However, in the SAB,

when the GS flows closer to the coast, the shape of the continental shelf and slope can significantly alter the flow (Fig. 3c, d). In particular, flow is enhanced along slopes, so stronger flow along the shelf break is noted in the realistic model.

3.2 The tilt of mean sea level along the coast

The change of mean sea level along the coast and the sea level variability due to variations in the zonal wind are shown in Fig. 4. The model results are compared with the geodetic models of sea level tilt used in Higginson et al. (2015). The mean sea level tilt along the coast is generally in agreement with the Higginson et al.'s results (Fig. 4a, b). Note, however, that compared with the Higginson's data, the difference in sea level between the MAB and SAB is underestimated in the

Fig. 3 Examples of velocity (in m s^{-1}) cross sections for the same runs as in Fig. 2. *Left and right panels* are for the NOVAR-S and NOVAR-R cases, respectively; *top and bottom panels* are for north-south section of *U* component along longitude 73°W (in MAB) and east-west section of *V* component along latitude 31°N (in SAB), respectively. *White and black contours* represent negative and positive values, respectively
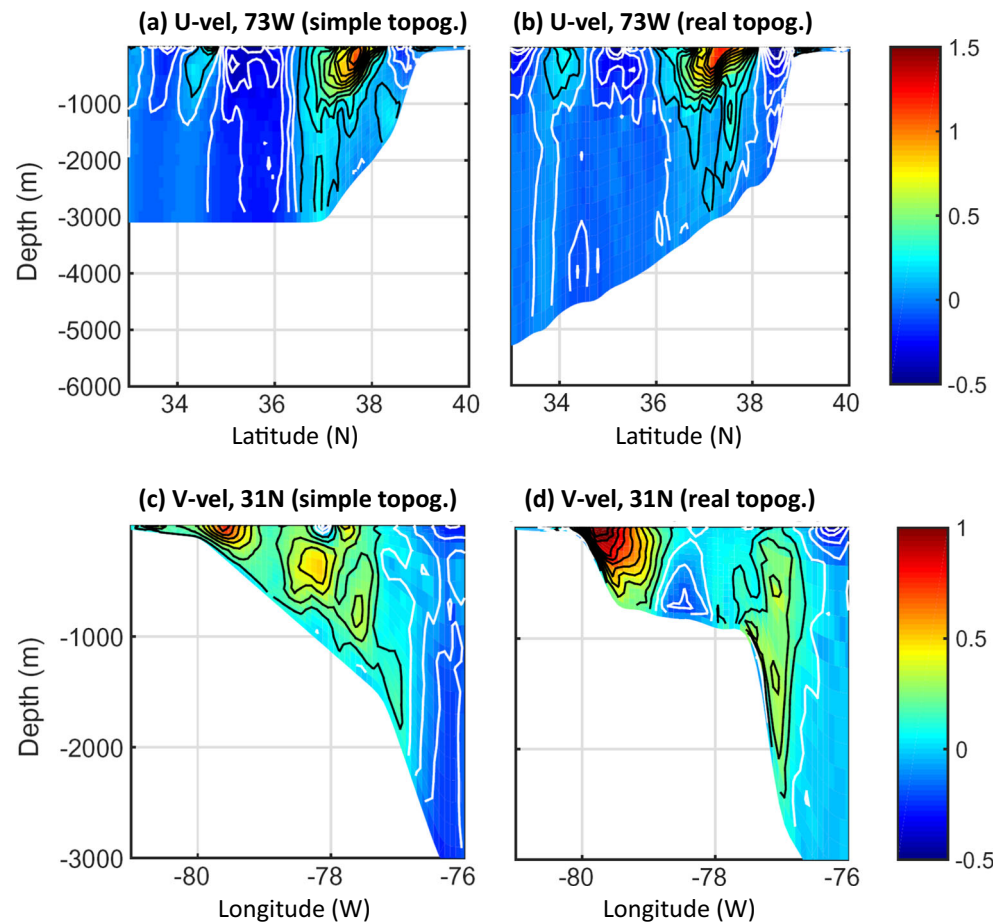

simplified model (Fig. 4a) and overestimated in the realistic model (Fig. 4b). The geodetic calculations were done for only three locations in the SAB that overlap the ocean model, so more quantitative comparison is not possible. The most interesting result is that the difference in mean sea level between the middle of the SAB (say at 30°N) and the middle of the MAB (say at 40°N) is ~10 cm in the case of simple topography, while this difference is ~22 cm in the case of realistic topography. The topography has the largest impact in the SAB and in particular near Cape Hatteras; in NOVAR-S the mean sea level tilt in the SAB is gradual, while in NOVAR-R the tilt is abrupt near Cape Hatteras. This difference may have implications for coarse resolution models that do not resolve the details of the coastline.

In the control experiments with constant forcing (NOVAR), sea level variability along the coast (green lines) is relatively small, ~1–3 cm (Fig. 4a, b), and the variability is internally generated by the natural meandering of the GS. The model variability in this case maybe underestimated because of the model setting of fixed GS outflow location and no time-dependent forcing. When adding forced variations of ±5 m s^{-1} in the zonal wind (WINDVAR), sea level variability is larger, ~5–15 cm (Fig. 4c, d). With more realistic topography (Fig. 4d), the sea level variability in the SAB increased by a

factor of 2 compared with the simple topography case (Fig. 4c) due to the more realistic shelf (Fig. 3c, d), and the variability is more irregular in the MAB due to the additions of bays and estuaries. Recent studies support the notion that the response of CSL to variations in the wind may be different for the SAB and the MAB (Piecuch et al. 2016; Woodworth et al. 2016), as demonstrated also here.

Figure 5 shows that the mean sea level tilt is quite robust in the realistic topography case (blue lines in Figs. 4b and 5b are quite similar), but in the idealized topography case, the variable forcing reduces the tilt compared with a constant forcing case (Fig. 4a versus Fig. 5a). The results suggest that the dynamic adjustment of the mean sea level may be affected by both topography and forcing that influence large-scale and coastal waves during the adjustment process. The CSL variability (around ~5–10 cm) that is driven by the imposed GS variability is different for each case. CSL variability seems sensitive to both topography (left vs. right panels in Fig. 5) and inflow source (top vs. bottom panels in Fig. 5). The largest and most coherent CSL variability is found when imposed variations of ±10 Sv are applied on the GS through variations in the Florida Current transport and when a model with simple topography is used (Fig. 5a). In this case, large-scale barotropic signals along the length of the GS generate coastal-trapped
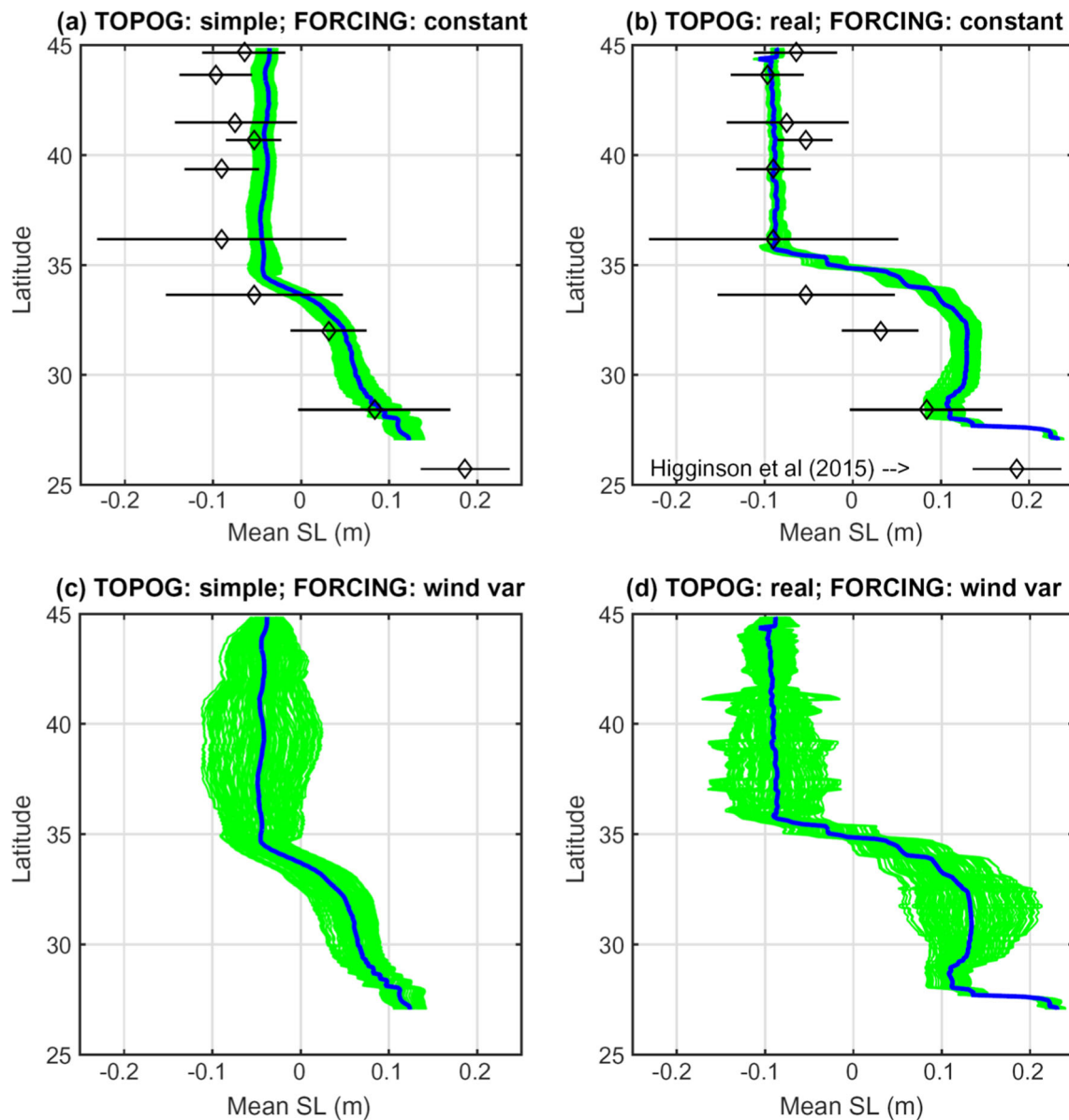
Fig. 4 North-south variations of sea level along the coast; *green lines* are values every 6 h, and the heavy *blue line* is the mean value over 50 days for each case. *Top panels* are for cases with constant forcing: **a** NOVAR-S and **b** NOVAR-R; *black diamonds and horizontal bars* are the mean and standard deviation of 7 geodetic models (data from Higginson et al. 2015). *Bottom panels* are for cases with oscillating wind forcing: **c** WINDVAR-S and **d** WINDVAR-R

waves and coherent CSL variations, as shown by Ezer (2016b). It is likely though that the simultaneously imposed fluctuations in both ends of the model GS contribute to making the GS variations and coastal responses more coherent than in the real ocean. Introducing a source only in the north through the Slope Current inflow reduces the variability (Fig. 5c). When more realistic topography is used, the variability is significantly reduced in the MAB when the forcing is the FC (e.g., Fig. 5b vs. Fig. 5a). Apparently, the sharp coastal corner at Cape Hatteras may have impact on coastal waves connecting the SAB and the MAB. A somewhat peculiar result is the fact that when the source of transport variability is from the north (SC), the variability in the lower MAB

increases (Fig. 5d) which suggests that a north source may be a more efficient way to generate southward propagating coastal waves; this will be discussed later. In any case, the experiments demonstrate quite clearly the important role that the topography plays in both the mean sea level tilt and its variability.

3.3 Gulf Stream's induced coastal sea level variability

The focus is now shifted to the time-dependent CSL variations induced by the GS. When the GS variability is imposed by variations in the inflow transport of the FC over the simple topography model (FCVAR-S case in Table 1), CSL
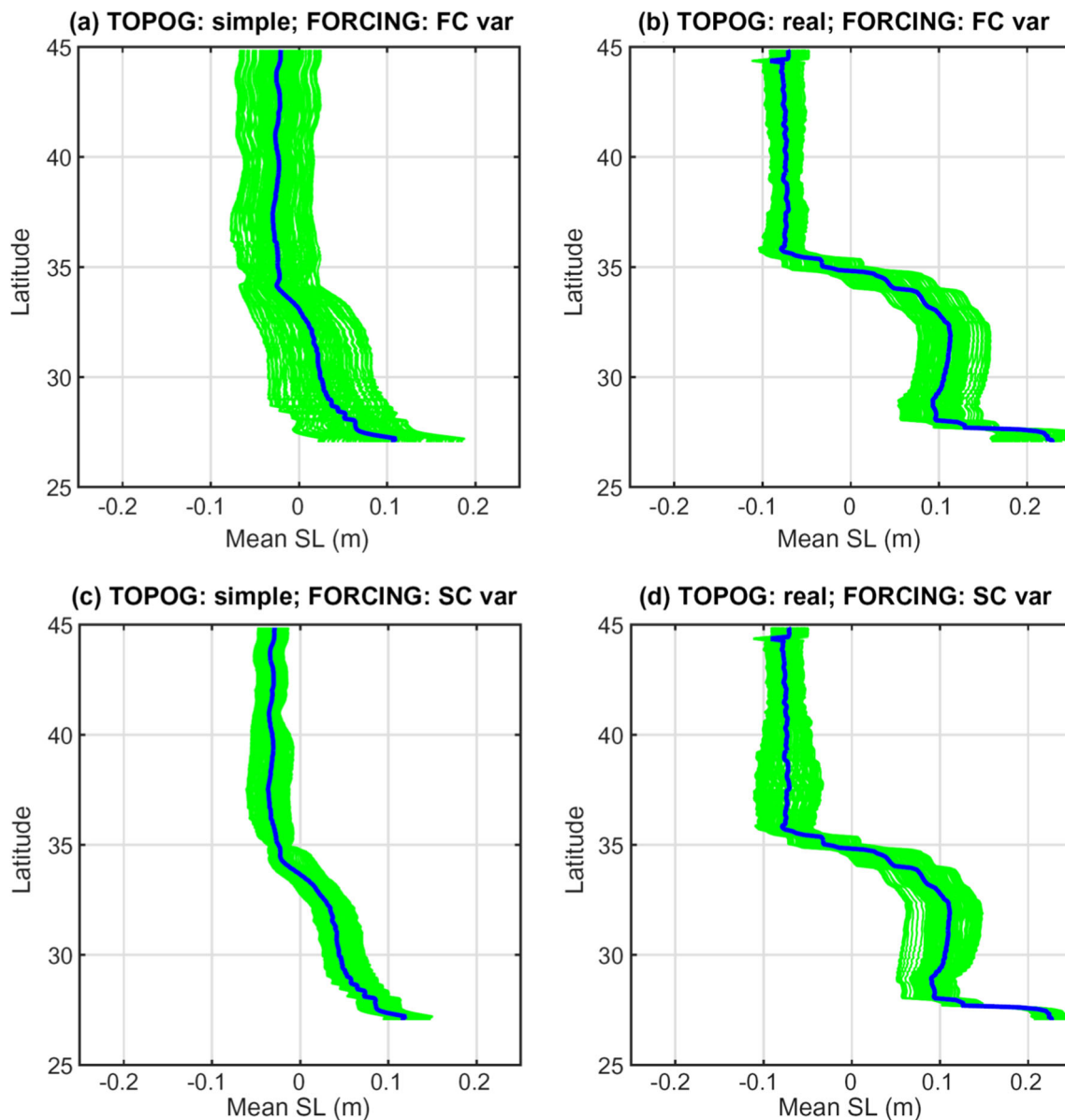
Fig. 5 Same as Fig. 4, but for cases with variable Gulf Stream forced by oscillations in the Florida Current (**a** FCVAR-S and **b** FCVAR-R) and the Slope Current (**c** SCVAR-S and **d** SCVAR-R)

variations are very coherent along the US East Coast (Fig. 6a); this is the same case as in Ezer (2016b). When using a realistic topography (FCVAR-R; Fig. 6b), there are larger differences in CSL variability and mean sea level between the SAB (blue-shed lines) and the MAB (red-shed lines). In particular, internally induced variability with periods of ~20 days (compared with the 5-day-cycle imposed variability) is evident in the SAB (closer to the FC inflow), but less so in the MAB (Fig. 6b). When the source of GS variability in the realistic model is coming from the north through transport variations in the SC (SCVAR-R; Fig. 6d), CSL variations are quite similar to those forced by the FC (Fig. 6b). Note however, that the response of CSL to SC forcing is in opposite phase to the response of CSL to FC forcing, i.e., when stronger westward

SC flow enters the model from the east, coastal sea level is rising, while when stronger northward FC flow enters the model from the south, coastal sea level is falling. This result is consistent with the geostrophic balance across the GS and the SC as seen in the sea level slopes (in Fig. 2b, when moving northward sea level slopes downward across the "Gulf Stream," then upward across "N. Recir.," which is the northern recirculation driven by the SC). The odd case that looks different from the other experiments is when SC inflow variations are imposed on the simple topography model (SCVAR-S; Fig. 6c). In this case, the high-frequency variations in the MAB are smaller and the variations in the SAB are mostly the internal 20-day cycles, not the 5-day imposed ones. It seems that the less-defined continental shelf in the smooth
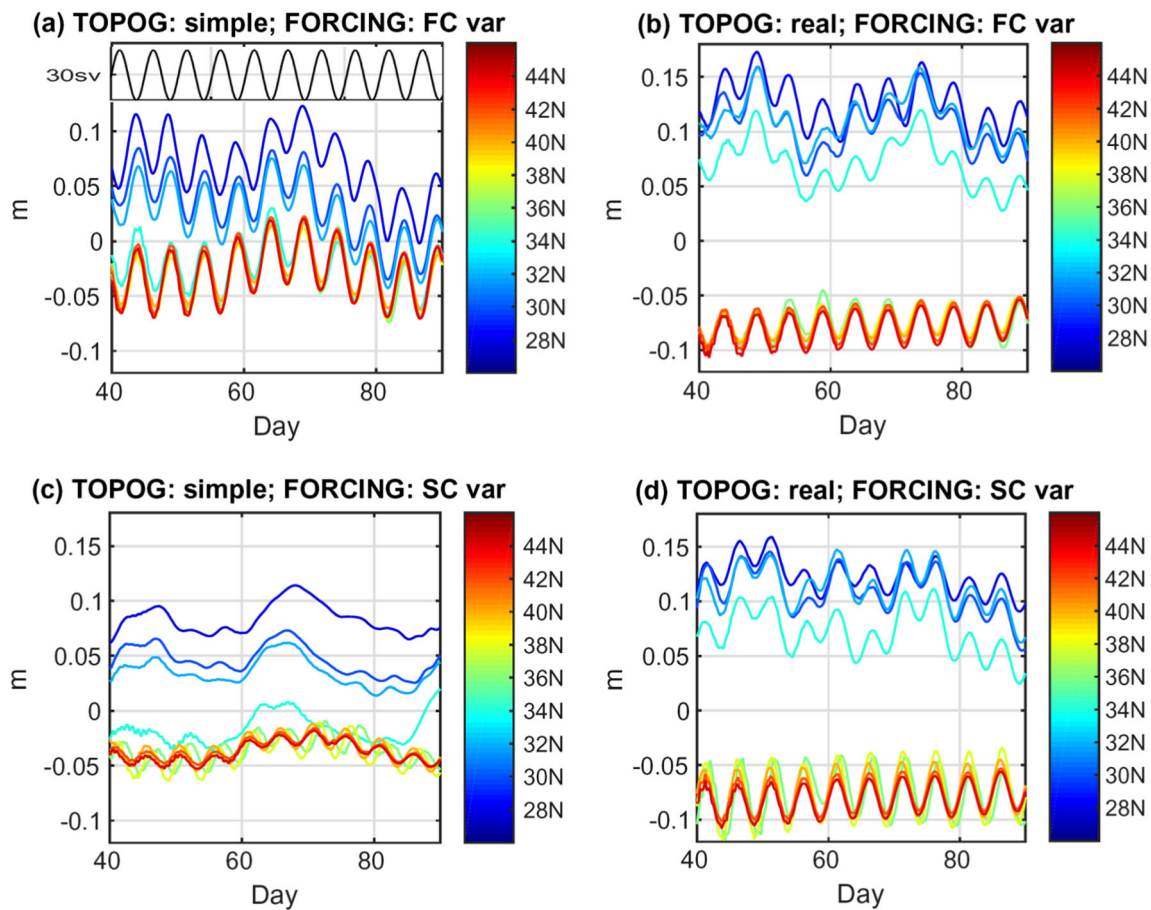
Fig. 6 The time variations in CSL at different locations (from 28°N to 44°N in *blue to red colors*) for the same cases as Fig. 5. The imposed Florida Current transport (30 ± 10 Sv) is shown in *black* on the top of (**a**); forcing is identical for (**b**), but for (**c**) and (**d**), the same pattern represents the absolute SC transport of 40 ± 10 Sv (however, imposed FC direction is northward and imposed SC direction is westward)

topography (Fig. 3c) depresses the southward propagation of coastal-trapped waves. The transmitting of large-scale signals into a coastal signal through the generation of coastal-trapped waves is sensitive to the shape of the continental slope and to the frequency of the signal (Huthnance 2004) and can result in coherent sea level variability along many different coasts (Hughes and Meredith 2006). In particular, for some frequencies, coastal signals are depressed or amplified, as demonstrated in Ezer (2016b), and apparently the difference in topography between the simple and realistic cases is responsible for the different response between Fig. 6c and Fig. 6d.

To look at potential signal propagation, the sea level along the coast as a function time and latitude is shown in the so-called Hovmöller diagram in Fig. 7 for the same four cases as in Fig. 6. The large jump in the mean sea level between the SAB (mostly red) and MAB (mostly blue) is again evident in the realistic cases (right panels of Fig. 7), as discussed before. In the cases where the imposed forcing is the inflow of the FC transport (upper panels of Fig. 7), the oscillations are more coherent and simultaneously occurring along the coast, indicating a response associated with the fast-moving barotropic waves that originate near

the GS and propagate in deep water toward the coast. As noted before, the fact that the GS in the model is forced simultaneously on both ends contributes for this coherent CSL response. On the other hand, when the imposed variability originates in the north by the SC transport (lower panels of Fig. 7), the oscillations seem to propagate southward along the coast, reaching the entire coast in SCVAR-R, but remaining in the MAB in SCVAR-S (due to the lack of shelf, as discussed before). Ezer (2016b) also noted that forcing the entire GS by variations in the FC tends to produce a barotropic response, while forcing from the north by the SC generates equatorward propagating coastal waves that move slower, close to the speed of baroclinic shelf waves. Figure 8 focuses on the MAB in the SCVAR-R case (an enlarged portion of Fig. 7d) during a 2-week period. In the lower MAB, there is clear southward propagation of sea level signal, as expected from coastal waves in the northern hemisphere (Huthnance 2004). The propagation speed in Fig. 8 is estimated as ∼7 m s^{-1}. By comparison, a frictionless barotropic coastal Kelvin wave at the model's shallowest points (10 m) would propagate at a speed of ∼10 m s^{-1}.
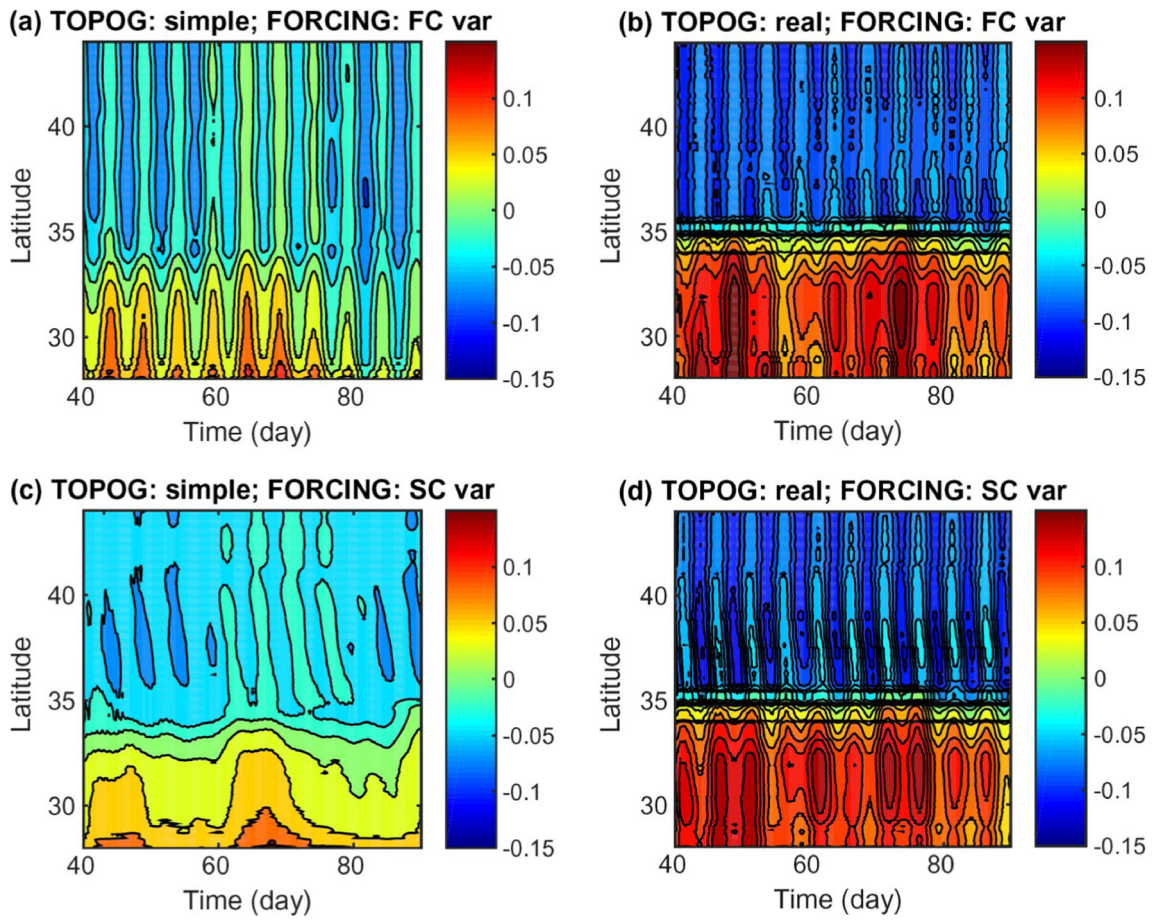
Fig. 7 Hovmöller diagram of CSL (color in m) as a function of time and latitude along the coast for the same cases as Figs. 5 and 6

Fig. 8 Enlarged Hovmöller diagram focusing on the MAB area during a 2-week period (same SCVAR-R case as in Fig. 7d)
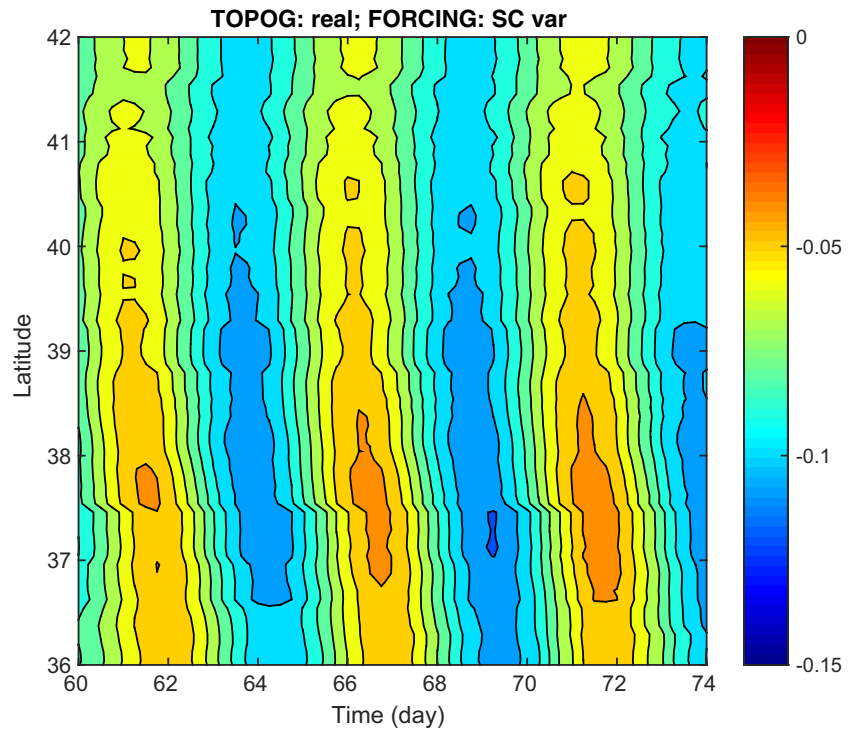
3.4 Correlation of coastal sea level with the Gulf Stream

The idealized model experiments conducted here show very coherent coastal sea level response when the imposed GS oscillations are the only time-dependent forcing (in reality, when other local forcing such as wind, waves, and tides are included, CSL coherency is expected to be reduced). Figure 9 shows the spatial pattern of the correlation between sea level and FC transport. The 5-day-period sinusoidal forcing is such

that when FC transport is minimum/maximum, CSL is maximum/minimum (Fig. 6a). It appears that coherent significant negative correlations extend for all the continental shelf from the coast to at least 100 m depth and in the MAB to ~1500 m; this result may not be surprising given the fact that except the GS, no other time-dependent forcing (such as wind, air pressure, rivers, and tides) exists here. Positive correlations occupy the region south and east of the GS. Variations in the FC transport seem part of coherent sea level signals along the

Fig. 9 Correlation coefficient between sea surface height and FC transport for cases **a** FCVAR-R and **b** FCVAR-S. The calculations are for 6-hourly data of days 40–90 (as in Fig. 6). The correlation is statistically significant at 99% confidence for most of the domain, except a narrow band along the GS front. The contour interval for correlation is 0.1 with *blue/red* representing values of −1/+1. Bottom topography contours (*white lines*) are shown for depths of 100, 1500, 3000, and 4500 m

(a) FC-sea level correlation (realistic topography)

(b) FC-sea level correlation (simple topography)
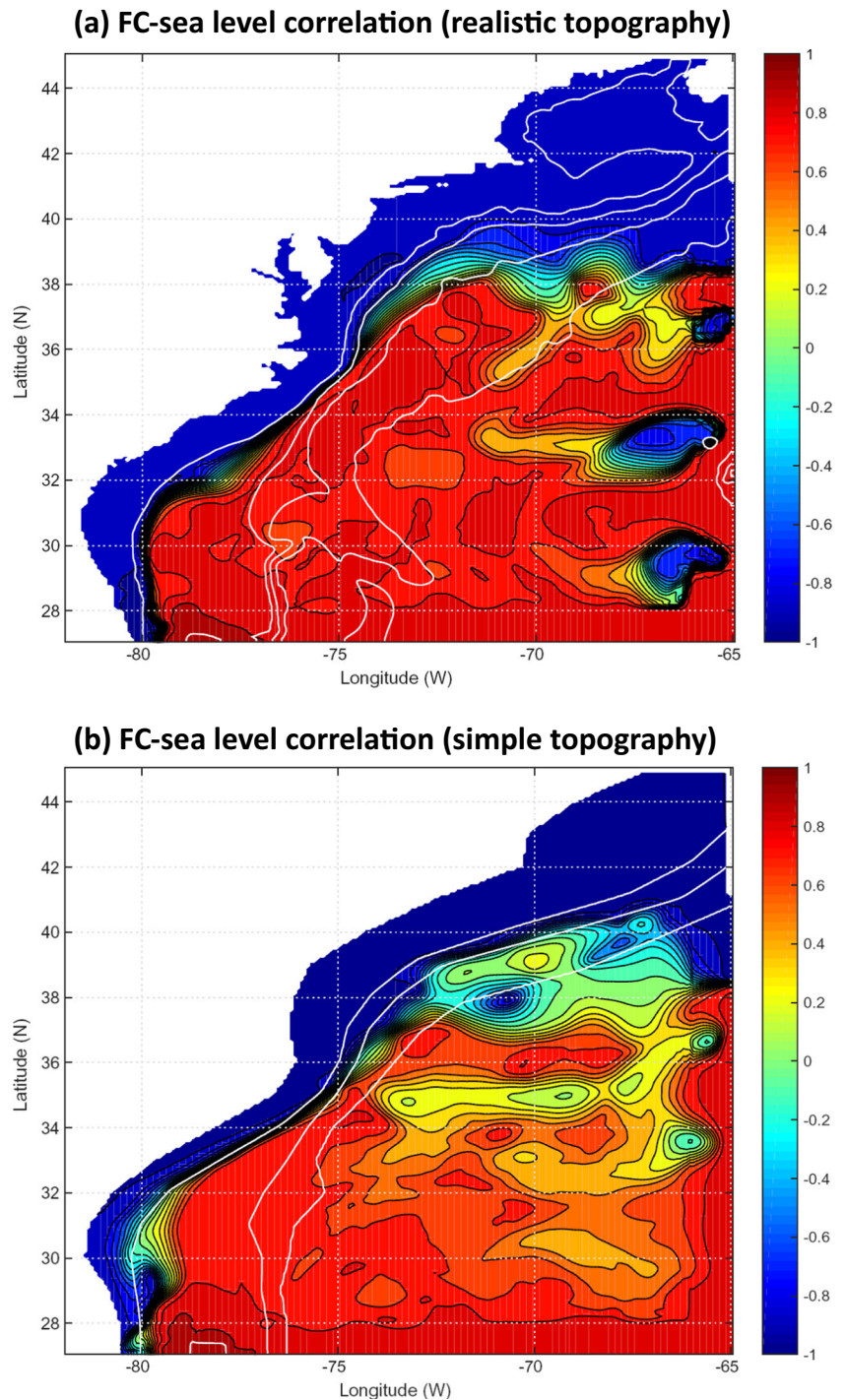
path of the GS farther downstream; this result is seen also in other models (e.g., see the similarity between Figure 4c in Zhao and Johns 2014 and Fig. 9 here). The important implication of this result is that the FC measurements may represent large portion of the GS variability downstream (which are not directly observed). There are however differences between the case with realistic topography (Fig. 9a) and the case with simple topography (Fig. 9b), which highlights the role of topography in generating sea level variability. In the SAB, the impact of the Charleston Bump on the deflection of the GS is clearly seen around 32°N, 78°W, but only in the model with realistic topography. The ability of this topographic feature to generate coastal variations when interacting with the GS has been indicated in observations and models (Oey et al. 1992). In the simple topography case, there is some anomaly around 29°N, possibly due to the FC boundary conditions, and some local anomalies near the eastern boundary are seen in the case with realistic topography, possibly due to interaction with Bermuda and other deep ocean features. There is also a difference in the correlations in the MAB, especially in the northern recirculation gyre region between the GS and the continental slope, where SC-topography interactions are important (Ezer 2016a). The homogeneous positive/negative correlations south/north of the GS clearly indicate that the simultaneous oscillating boundary conditions of FC inflow and GS outflow have impact along the entire GS path. This idealized model configuration may create a more coherent CSL response (FC-CSL correlations of ~0.6–1.0) than in the real ocean, but observations in fact also show statistically significant FC-CSL correlations (~0.4–0.6) from the SAB and MAB all the way to the Gulf of Maine (see Figure 1 in Ezer 2016b). However, observations also show a little larger lag between the FCT and CSL (but still quite an immediate CSL-GS relation within hours not days). The general pattern of CSL correlation with SC (not shown) is quite similar to Fig. 9, except that the negative correlation along the coast means that stronger negative SC (southwestward flowing coastal current) is correlated with higher CSL, while stronger FC (northeastward flowing GS) is correlated with lower CSL.

4 Summary and conclusions

The study addresses the interaction of the GS with bottom topography and the coastline, with emphasis on the impact of this interaction on coastal sea level variability along the US East Coast. Both the short-term temporal variability and the spatial sea level change along the coast are investigated using an idealized regional numerical ocean model. Comparisons between model simulations with a simplified topography and simulations with a realistic topography demonstrate how the topography affects the coastal sea level variability. The main motivation for this study comes from

renewed interest in the impact of remote variations in the Atlantic Ocean circulation, and the GS in particular, on coastal sea level variability (Ezer 2001, 2013, 2015, 2016b; Ezer et al. 2013; Goddard et al. 2015; Domingues et al. 2016). One should acknowledge though that even before the age of realistic ocean modeling and satellite altimetry, some early observations indicate a possible link between coastal processes (such as CSL) and variations in the GS (Montgomery 1938; Blaha 1984). Other early studies also show how the GS can influence coastal dynamics, for example, by GS intrusion into shallow regions (Atkinson 1977) and by GS position change that can affect coastal currents (Bane et al. 1988). These complex GS-coastal dynamic relations can now be studied with the help of numerical ocean models. The current study is a follow up on the recent modeling study of Ezer (2016b) which used a simplified regional model (as in Fig. 1b) to demonstrate that variations in the GS transport (with periods of 2–10 days) are related to coherent CSL variations similar to what have seen in observations. Fast-moving barotropic waves are induced by the GS variability and generate coastal-trapped waves that distribute the signal along the coast. This connection can be used to predict tidal flooding in the MAB from changes in the FC transport (Ezer and Atkinson 2014) as monitored by the long observations from the cable across the Florida Straits (Baringer et al. 2001). The amplitude of CSL variability driven by GS variations of ± 10 Sv is generally similar to CSL variability driven by zonal wind variations of ± 5 m s^{-1}. Here, the simulations of Ezer (2016b) have been compared with simulations using a more realistic topography. The results show that with a more realistic topography, there are larger differences in the CSL variability between the SAB and MAB. The shape of the topography (in particular, the continental shelf and slope) affects the propagation of coastal waves, as suggested by theoretical and process studies of coastal-trapped waves (Huthnance 2004). Therefore, GS-induced CSL variability is also affected by the details of the local topography.

In addition to studying the GS-related high-frequency CSL variability, the study also found interesting results applicable to another issue of long history (and some controversy): the north-south tilt of mean sea level along the coast (Sturges 1974). The latter issue received a renewed interest by the study of Higginson et al. (2015), who analyzed several geodetic and ocean models to settle some past disagreements between geodetic observations and ocean dynamics. However, the role of topography and the discrepancy between different models are not completely understood; in particular, the impact of the sharp change in topography near Cape Hatteras on the sea level differences between the SAB and the MAB is explored here. The model with simple topography may resemble to some degree the topography in coarse resolution models that do not resolve the details of the sharp coastline shape at Cape Hatteras or the details of the continental

shelf topography. The results demonstrate that the detailed topography near Cape Hatteras can contribute to the sharp downward slope of mean sea level, resulting in a larger difference between the high coastal sea level in the SAB and the lower coastal sea level in the MAB. The model with an idealized smoothed topography shows a SAB-MAB sea level difference that is smaller by about a factor of 2 than that obtained by the realistic model. It appears that the intensification of the GS when it separates from the coast is strongly affected by the local topography, a result consistent with recent studies of the GS separation problem (Ezer 2016a; Schoonover et al. 2017). The implication is that coarse resolution models that do not resolve the topography very well may underestimate the tilt of mean sea level along the coast. Sea level rise associated with climate-related weakening of the Gulf Stream (Ezer et al. 2013) may also be affected by this topographic effect. Therefore, coarse resolution climate models intended to project spatial variations in coastal sea level and local sea level rise projections should pay more attention to coastal features such as capes. Potential improvements to such models may include refining or adjusting topographic features of particular importance such as Cape Hatteras. Parameterizations of model flows near critical topographic features can also be considered, as has been done, for example, for improving overflow dynamics in climate models that do not resolve narrow straits (Legg et al. 2009).

References

Atkinson LP (1977) Modes of Gulf Stream intrusion into the South Atlantic Bight shelf waters. Geophys Res Lett 4(12):583–586

Bane JM, Brown OB, Evans RH, Hamilton P (1988) Gulf Stream remote forcing of shelfbreak currents in the Mid-Atlantic Bight. Geophys Res Lett 15(5):405–407

Baringer MO, Larsen JC (2001) Sixteen years of Florida current transport at 27N. Geophys Res Lett 28(16):3,179–3,182

Blaha JP (1984) Fluctuations of monthly sea level as related to the intensity of the Gulf Stream from Key West to Norfolk. J Geophys Res Oceans 89(C5):8033–8042

Boon JD (2012) Evidence of sea level acceleration at U.S. and Canadian tide stations, Atlantic coast, North America. J Coast Res 28(6):1437–1445. doi:10.2112/JCOASTRES-D-12-00102.1

Domingues R, Baringer M, Goni G (2016) Remote sources for year-to-year changes in the seasonality of the Florida Current transport. J Geophys Res. doi:10.1002/2016JC012070

Ducet N, Le Traon PY, Reverdin G (2000) Global high-resolution mapping of ocean circulation from TOPEX/Poseidon and ERS-1 and -2. J Geophys Res 105(C8):19477–19498. doi:10.1029/2000JC900063

Ezer T (1994) On the interaction between the Gulf Stream and the New England Seamount Chain. J Phys Oceanogr 24:191–204. doi:10.1175/1520-0485(1994)024

Ezer T (2001) Can long-term variability in the Gulf Stream transport be inferred from sea level? Geophys Res Lett 28(6):1031–1034. doi:10.1029/2000GL011640

Ezer T (2013) Sea level rise, spatially uneven and temporally unsteady: why the U.S. East Coast, the global tide gauge record, and the global altimeter data show different trends. Geophys Res Lett 40:5439–5444. doi:10.1002/2013GL057952

Ezer T (2015) Detecting changes in the transport of the Gulf Stream and the Atlantic overturning circulation from coastal sea level data: the extreme decline in 2009-2010 and estimated variations for 1935-2012. Glob Planet Change 129:23–36. doi:10.1016/j.gloplacha.2015.03.002

Ezer T (2016a) Revisiting the problem of the Gulf Stream separation: on the representation of topography in ocean models with different types of vertical grids. Ocean Model 104:15–27. doi:10.1016/j.ocemod.2016.05.008

Ezer T (2016b) Can the Gulf Stream induce coherent short-term fluctuations in sea level along the U.S. East Coast?: a modeling study. Ocean Dyn 66(2):207–220. doi:10.1007/s10236-016-0928-0

Ezer T, Atkinson LP (2014) Accelerated flooding along the U.S. East Coast: on the impact of sea-level rise, tides, storms, the Gulf Stream, and the North Atlantic oscillations. Earth's Future 2(8):362–382. doi:10.1002/2014EF000252

Ezer T, Atkinson LP, Corlett WB, Blanco JL (2013) Gulf Stream's induced sea level rise and variability along the U.S. mid-Atlantic coast. J Geophys Res 118:685–697. doi:10.1002/jgrc.20091

Goddard PB, Yin J, Griffies SM, Zhang S (2015) An extreme event of sea-level rise along the Northeast coast of North America in 2009–2010. Nat Commun 6. doi:10.1038/ncomms7346

Higginson S, Thompson KR, Woodworth PL, Hughes CW (2015) The tilt of mean sea level along the east coast of North America. Geophys Res Lett 42(5):1471–1479. doi:10.1002/2015GL063186

Hogg NG (1992) On the transport of the Gulf Stream between Cape Hatteras and the Grand Banks. Deep-Sea Res 39(7–8):1231–1246. doi:10.1016/0198-0149(92)90066-3

Hughes CW, Meredith PM (2006) Coherent sea-level fluctuations along the global continental slope. Philos Trans R Soc 364:885–901. doi:10.1098/rsta.2006.1744

Huthnance JM (2004) Ocean-to-shelf signal transmission: a parameter study. J Geophys Res 109(C12029). doi:10.1029/2004JC002358

Johns WE, Shay TJ, Bane JM, Watts DR (1995) Gulf Stream structure, transport, and recirculation near 68°W. J Geophys Res 100:817–817

Larnicol G, Guinehut S, Rio MH, Drévillon M, Faugere Y, Nicolas G (2006) The global observed ocean products of the French Mercator Project. Proceedings of the Symposium on 15 Years of Progress in Radar Altimetry, Edited by Danesy D, ISBN:92-9092-925-1. Noordwijk, Netherlands, European Space Agency, id.110

Legg S, Chang Y, Chassignet EP, Danabasoglu G, Ezer T, Gordon AL, Griffies S, Hallberg R, Jackson L, Large W, Ozgokmen T, Peters H, Price J, Riemenschneider U, Wu W, Xu X, Yang J (2009) Improving oceanic overflow representation in climate models: the Gravity Current Entrainment Climate Process Team. Bull Amer Met Soc 90(5):657–670. doi:10.1175/2008BAMS2667.1

Mellor GL, Hakkinen S, Ezer T, Patchen R (2002) A generalization of a sigma coordinate ocean model and an intercomparison of model vertical grids. In: Pinardi N, Woods ED (eds) Ocean forecasting: conceptual basis and applications. Springer, pp 55–72. doi:10.1007/978-3-662-22648-3_4

Montgomery R (1938) Fluctuations in monthly sea level on eastern U.S. Coast as related to dynamics of western North Atlantic Ocean. J Mar Res 1:165–185

Oey LY, Ezer T, Mellor GL, Chen P (1992) A model study of "bump" induced western boundary current variabilities. J Mar Sys 3:321–342. doi:10.1016/0924-7963(92)90009-W

Piecuch CG, Ponte RM (2015) Inverted barometer contributions to recent sea level changes along the northeast coast of North America. Geophys Res Lett 42(14):5918–5925. doi:10.1002/2015GL064580

Piecuch C, Dangendorf S, Ponte R, Marcos M (2016) Annual sea level changes on the North American Northeast Coast: influence of local winds and barotropic motions. J Clim 29:4801–4816. doi:10.1175/JCLI-D-16-0048.1

Richardson PL, Knauss JA (1971) Gulf Stream and western boundary undercurrent observations at Cape Hatteras. Deep-Sea Res 18(11):1089–1109. doi:10.1016/0011-7471(71)90095-7

Rossby T, Flagg C, Donohue K (2010) On the variability of Gulf Stream transport from seasonal to decadal timescales. J Mar Res 68:503–522

Sallenger AH, Doran KS, Howd P (2012) Hotspot of accelerated sea-level rise on the Atlantic coast of North America. Nature Clim Change 2:884–888. doi:10.1038/NCILMATE1597

Schoonover J, Dewar WK, Wienders N, Deremble B (2017) Local sensitivities of the Gulf Stream separation. J Phys Oceanogr 47(2). doi:10.1175/JPO-D-16-0195.1

Sturges W (1974) Sea level slope along continental boundaries. J Geophys Res 79(6):825–830. doi:10.1029/JC079i006p00825

Thompson PR, Mitchum GT (2014) Coherent sea level variability on the North Atlantic western boundary. J Geophys Res 119(9):5676–5689. doi:10.1002/2014JC009999

Woodworth PL, Maqueda MAM, Roussenov VM, Williams RG, Hughes CW (2014) Mean sea-level variability along the northeast American Atlantic coast and the roles of the wind and the overturning circulation. J Geophys Res 119:8916–8935. doi:10.1002/2014JC010520

Woodworth PL, Maqueda MM, Gehrels WR, Roussenov VM, Williams RG, Hughes CW (2016) Variations in the difference between mean sea level measured either side of Cape Hatteras and their relation to the North Atlantic Oscillation. Clim Dyn:1–19. doi:10.1007/s00382-016-3464-1

Xu F-H, Oey L-Y (2011) The origin of along-shelf pressure gradient in the Middle Atlantic Bight. J Phys Oceanogr 41(9):1720–1740. doi:10.1175/2011JPO4589

Yin J, Goddard PB (2013) Oceanic control of sea level rise patterns along the East Coast of the United States. Geophys Res Lett 40:5514–5520. doi:10.1002/2013GL057992

Zhao J, Johns W (2014) Wind-forced interannual variability of the Atlantic Meridional Overturning Circulation at 26.5°N. J Geophys Res Oceans 119:6253–6273. doi:10.1002/2013JC009407